Stability Analysis of Carbon Nanotube Interconnects

Mekala Girish Kumar, Yash Agrawal and Rajeevan Chandel

Abstract This paper deals with frequency and stability response of single wall carbon nanotube bundle (SWB) and multiwall carbon nanotube bundle (MWB) at global interconnect lengths. The performance of SWB and MWB interconnects are analyzed using driver-interconnect-load system. It is analyzed that MWB interconnects are more stable than SWB interconnects. It is illustrated that stability of both SWB and MWB interconnects increases with increase in interconnect length. The analytical model for stability and frequency response using *ABCD* matrix has been formulated. Using frequency response, it is observed that the bandwidth of SWB and MWB interconnects are 7.94 and 22.2 GHz respectively for an interconnect length of 500 μm. The results are verified using SPICE simulations. The time delay analysis has been performed for different interconnect lengths. Further, it is investigated that delay reduces with increasing number of shells in MWB interconnect.

Keywords Carbon nanotubes (CNT) · Kinetic inductance · MWCNT · Quantum resistance · Quantum capacitance · SWCNT

1 Introduction

In VLSI technology, the chip performance and signal integrity is dependent on interconnect delay in deep submicron technology (DSM) [1]. As technology scales down interconnects are a major concern as these degrades system performance and

M.G. Kumar (✉) · Y. Agrawal · R. Chandel
Electronics and Communication Engineering, National Institute of Technology Hamirpur, Hamirpur, Himachal Pradesh, India
e-mail: giri.frds@gmail.com

Y. Agrawal
e-mail: mr.yashagrawal@gmail.com

R. Chandel
e-mail: rchandel@nith.ac.in

P. Deiva Sundari et al. (eds.), *Proceedings of 2nd International Conference on Intelligent Computing and Applications*, Advances in Intelligent Systems and Computing 467, DOI 10.1007/978-981-10-1645-5_2

causes reliability problems. With scaling technology, grain boundary and surface scattering phenomenon increases in copper interconnects [2]. At high frequencies, issues like skin effect, operational bandwidth and stability response affect the performance of copper interconnects [3]. To overcome these limitations, the carbon nanotubes (CNT) have been proposed as potential materials for interconnect applications as these possess extremely long mean free path (MFP), large current capability [4]. CNTs are made by graphene sheet that are rolled up into cylindrical structure. CNTs are classified into single wall carbon nanotubes (SWCNTs) and multiwall carbon nanotubes (MWCNTs). SWCNTs are either metallic or semiconducting depending on their chirality [5]. But, MWCNTs are always metallic in nature [6]. Also, MWCNTs are easier to fabricate as compared to SWCNTs due to their growth process. The most promising material for global interconnects is MWCNTs due to its high current carrying capability than SWCNTs.

To analyze the performance of SWB and MWB interconnects for on-chip applications, frequency and stability response have been performed. It is important to note that stability and the frequency responses are affected by interconnect parameters, such as resistances, capacitances, and inductances.

Li et al. [7] have analyzed on-chip inductor design of CNTs at high frequencies. Nasiri et al. [8] derived input-output transfer function of a MWCNT using transmission line model. The stability and Nyquist plot for CNT bundle interconnect have been presented in Fathi et al. [9]. It is assumed that the driver parasitic and contact resistances are only for local interconnects.

This paper deals with stability and frequency response of CNT based interconnects. Rest of the paper is organized as follows. A brief description of SWB and MWB interconnect is presented in Sect. 2. In Sect. 3 transfer function and its analytical formulation is using driver-interconnect-load (DIL) system is presented. Stability and frequency domain analysis have been performed in Sect. 4. Finally, conclusions are drawn in Sect. 5.

2 Interconnect Model

This section presents a comprehensive analytical model for SWB and MWB interconnects. SWB and MWB of width (w), diameter (d) and thickness (t) is placed above the ground plane at a distance (h) as sown in Fig. 1.

The number of SWCNTs in a bundle as shown in Fig. 1a along x and y directions are expressed as [10]:

$$n_x = \frac{w - d}{sp} \tag{1}$$

$$n_y = \frac{2(t - d)}{\sqrt{3}sp} + 1 \tag{2}$$

where sp is inter-CNT distance of interconnect.

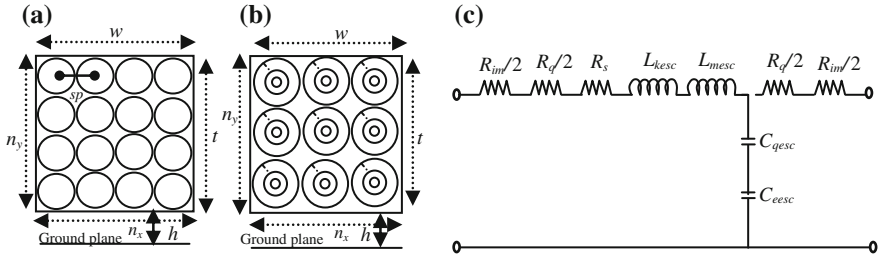

Fig. 1 **a** Cross sectional view of SWB. **b** MWB. **c** Equivalent single conductor model for SWB/MWB interconnect

Using (1) and (2), the total number of SWCNTs in bundle are given as

$$N_S = n_x n_y - \frac{n_y}{2} \quad if\ n_y\ is\ even \tag{3a}$$

$$N_S = n_x n_y - \frac{(n_y - 1)}{2} \quad if\ n_y\ is\ odd \tag{3b}$$

The number of MWCNTs in a bundle as shown in Fig. 1b along x and y directions are given as:

$$n_x = \frac{w - d_N}{d_N + \delta} + 1 \tag{4a}$$

$$n_y = \frac{2(t - d_N)}{\sqrt{3}(d_N + \delta)} + 1 \tag{4b}$$

Using (1) and (2), the total number of MWCNTs in bundle are given as

$$N_{MWCNT} = n_x n_y - \frac{n_y}{2} \quad if\ n_y\ is\ even \tag{5a}$$

$$N_{MWCNT} = n_x n_y - \frac{(n_y - 1)}{2} \quad if\ n_y\ is\ odd \tag{5b}$$

Figure 1c represents the equivalent single conductor model of SWB/MWB interconnects. The *RLC* parasitic values in the figure are calculated from Das and Rahaman [11].

3 Stability Analysis of SWB and MWB Interconnects

The transfer function (*TF*) of the SWB and MWB interconnect distributed line is derived to get the frequency and stability response at global interconnect lengths using DIL system.

The *TF* accurately considered the driver parasitics i.e. resistance (R_d) and capacitance (C_d) as shown in Fig. 2a. To obtain overall gain (V_o/V_i), the DIL system is represented as a cascaded connection of two-port networks as shown in Fig. 2b. Here, the two-port system is represented by *ABCD* parameters. The *ABCD* parameters of each of the two-port networks are denoted as f_1, f_2, f_3, f_4 and f_5. The Telegrapher's equation of distributed interconnect line is used to obtain *ABCD* matrix parameters f_4. Using the method, voltage and current at any point x of the DIL are expressed as [12, 13]

$$\frac{dV}{dx} = -(R_{esc} + sL_{esc})I(x) \tag{6}$$

$$\frac{dI}{dx} = -sC_{esc}.V(x) \tag{7}$$

To obtain overall gain, it is needed to evaluate transmission matrix (T_{final}) from Fig. 2b.

$$\begin{aligned} T_{final} = &\begin{bmatrix} 1 & R_d \\ 0 & 1 \end{bmatrix} \begin{bmatrix} 1 & 0 \\ {}_sC_d & 1 \end{bmatrix} \begin{bmatrix} 1 & R_{lump} \\ 0 & 1 \end{bmatrix} \\ &\times \begin{bmatrix} \cosh(\gamma px) & Z_0 \sinh(\gamma px) \\ 1/Z_0 \sinh(\gamma px) & \cosh(\gamma px) \end{bmatrix} \begin{bmatrix} 1 & R_{lump} \\ 0 & 1 \end{bmatrix} = \begin{bmatrix} A & B \\ C & D \end{bmatrix} \end{aligned} \tag{8}$$

The resultant transmission matrix of (8) can be obtained in terms of input and output parameters as

$$\begin{bmatrix} V_i \\ I_i \end{bmatrix} = \begin{bmatrix} A & B \\ C & D \end{bmatrix} \begin{bmatrix} V_0 \\ I_0 \end{bmatrix} \tag{9}$$

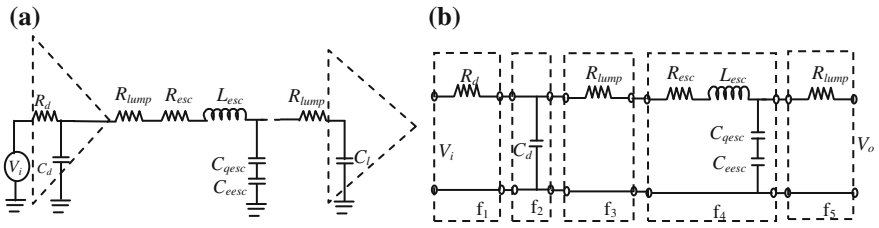

Fig. 2 **a** A driver-interconnect-load system. **b** Cascaded connections of the DIL of (**a**)

Thus, the *TF* is given as

$$TF = \frac{V_o}{V_i} = \frac{1}{A + sBC_l} \tag{10}$$

The parameters *A* and *B* of (10) are detailed in Appendix.

4 Results and Discussion

The Nyquist stability and frequency responses for SWB and MWB interconnects are evaluated using (10). The cross-sectional dimensions considered for interconnects are w = 48 nm and t = 144 nm. The parameters for 32 nm technology node are taken as per international technology road map (ITRS) [14]. The *RLC* values for SWB interconnect are 4.4 Ω/μm, 2.75 pH/μm, 14.97 aF/μm. The parasitic values for MWB interconnect are 1.6 Ω/μm, 2.17 pH/μm, 13.37 aF/μm. The driver resistance and capacitances are 13.8 KΩ and 0.07 fF respectively. The load capacitance (C_l) is 1 fF.

4.1 Stability Analysis

The Nyquist stability response of MWB for 500, 1000 and 2000 μm interconnect lengths is shown in Fig. 3a.

It is observed that for global interconnect lengths, the encirclement moves away from point (−1, 0) that interprets to higher system stability [15]. At the same time the Nyquist diagram imaginary values decrease leading to lower fluctuations in the system.

The Nyquist plot of SWB and MWB for an interconnect length of 1000 μm is shown in Fig. 3b. It is noticed that encirclement moves far away from point (−1, 0) for MWB interconnect as compared to SWB interconnect. This clearly states that MWB interconnects is more stable than SWB interconnects.

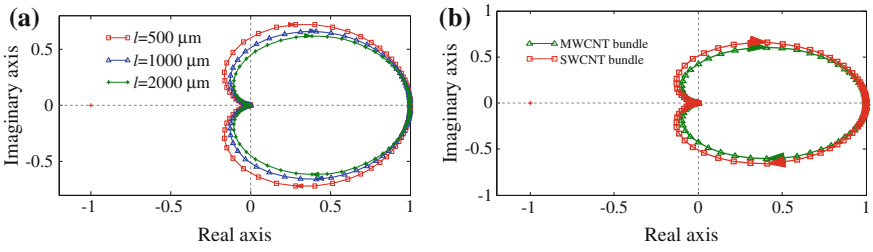

Fig. 3 **a** Nyquist plot for MWB interconnect at different interconnect lengths. **b** Nyquist plot for SWB and MWB interconnects

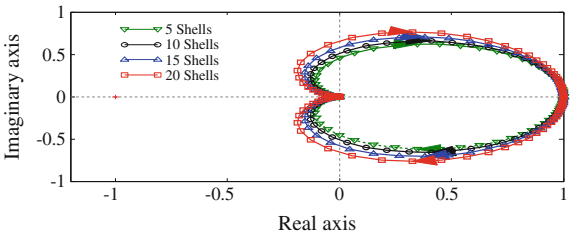

Fig. 4 Nyquist plot for MWB interconnect with different number of shells

The Nyquist response of MWB interconnects for 5, 10, 15 and 20 shells is shown in Fig. 4. As number of shells increases in MWCNT, the point (−1, 0) moves inside the encirclement. It is due to the number of shells increase in MWB interconnect, the damping coefficient (ξ) decreases. Higher quantitative value of ξmakes system becomes more stable.

4.2 Frequency Analysis

The open loop *TF* of (10) is used to analyze the frequency response of SWB and MWB interconnects. It is observed from Fig. 5a that MWB interconnect offers higher operating frequency as compared to SWB interconnect.

The cut off frequency for SWB and MWB interconnects are 7.8 and 22.2 GHz at interconnect length of 500 µm respectively.

Figure 5b plots the frequency response of MWB for different global interconnect lengths ranging from 500 to 2000 µm. It is noticed that operating frequency reduces for longer interconnects. It is observed from Fig. 5b, that SPICE simulation and analytical results are good in agreement. The average percentage error between SPICE and analytical results is 3.79 %.

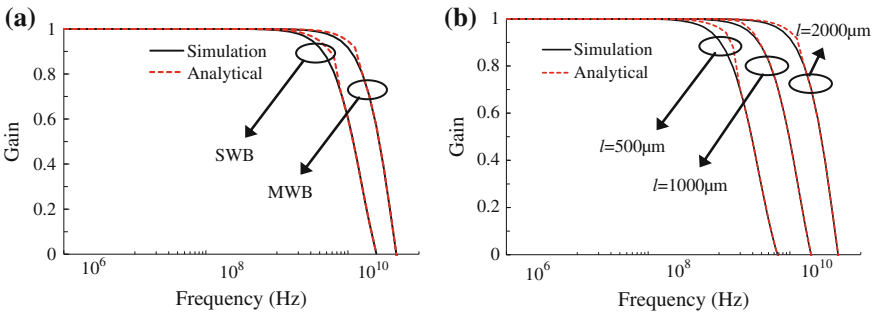

Fig. 5 **a** Frequency response of SWB and MWB interconnects. **b** Frequency response of MWB at different interconnect lengths

4.3 Delay Analysis

The time delay of SWB and MWB interconnects for different global interconnect lengths is shown in Fig. 6a. It is known that 50 % time delay (τ) for SWB and MWB interconnect can be obtained as the time it takes to reach 50 % of output voltage steady value [16],

$$\tau_{50\%} = \left(1.48 + e^{-2.9\xi^{1.35}}\right)\sqrt{L_{esc}l(C_{esc}l + C_l)} \tag{11}$$

where

$$\xi = 0.5\left(1 + \frac{C_l}{C_{esc}l}\right)^{-0.5}\left[\left(0.5R_{esc}l + 2R_{lump} + R_d\right)\sqrt{\frac{C_{esc}}{L_{esc}}} + \left(\mathrm{R}_{esc}l + 2R_{lump} + R_d\right)\sqrt{\frac{C_l^2}{L_{esc}C_{esc}l^2}}\right] \tag{12}$$

It is observed from Fig. 6a, that 50 % time delay (τ) of the DIL system of SWB and MWB at interconnect length 500 μm is 51.77 and 49.38 ps respectively. The delay calculated from SPICE simulation for SWB and MWB interconnects are 54.25 and 51.72 ps respectively. Thus the average error between analytical and simulation is 2.86 %.

Figure 6b shows that the delay of MWB with different number shells at global interconnect length ranging from 500 to 2500 μm. It is noticed that the delay reduces significantly with increasing number of shells.

The delays for 5 shells and 20 shells MWB interconnect for a length of 1000 μm are 96.1 and 98.4 ps respectively. The average error between simulative and analytic is 1.67 % and 2.34 % for 5 shells and 20 shells respectively.

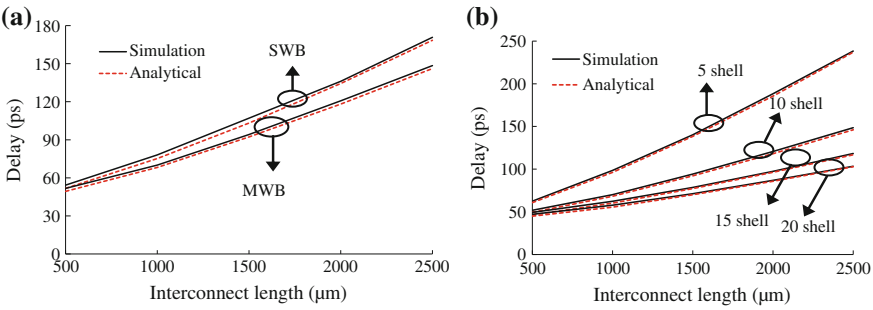

Fig. 6 **a** Time delay analysis of SWB and MWB at different interconnect lengths. **b** Time delay analysis of MWB with different number of shells

5 Conclusion

The present paper analyzes frequency and stability response of SWB and MWB interconnects. The driver interconnect load is considered. The interconnect is represented by equivalent ESC model for SWB/MWB interconnects. The transfer function is derived using *ABCD* model. At different global interconnect lengths, operating frequency and the 50 % time delay are computed for SWB/MWB interconnects. It is found that the MWB interconnect exhibits lesser time delay as compared to SWB interconnects. Further, it is observed that as the number of shells increases in MWB interconnect, the delay reduces substantially.

Appendix

$$A = 1 + s\left[\frac{R_{esc}C_{esc}(px)^2}{2} + R_dC_d + C_{esc}(px)\left(R_{lump} + R_d\right)\right] + s^2\left[\begin{array}{c}\frac{L_{esc}C_{esc}(px)^2}{2} + \frac{R_{esc}^2C_{esc}^2(px)^4}{24} \\ + \frac{R_{esc}R_dC_{esc}C_d(px)^2}{2} \\ + \frac{R_{esc}C_{esc}^2(px)^3\left(R_{lump}+R_d\right)}{6} + R_{lump}R_dC_dC_{esc}(px)\end{array}\right] \tag{A1}$$

$$B = \left(2R_{lump} + R_d + R_{esc}(px)\right) + s\left[\begin{array}{c}\frac{R_{esc}C_{esc}(px)^2}{2}\left(2R_{lump} + R_d\right) + 2R_{lump}R_dC_d + \frac{R_{esc}C_{esc}(px)^3}{6} \\ + L_{esc}(px) + R_{lump}^2C_{esc}(px) + R_{esc}R_dC_d(px) + R_{lump}R_dC_{esc}(px)\end{array}\right] \\ + s^2\left[\begin{array}{c}\left(2R_{lump} + R_d\right)\left(\frac{L_{esc}C_{esc}(px)^2}{2} + \frac{R_{esc}^2C_{esc}^2(px)^4}{24}\right) + R_{lump}R_dR_{esc}C_{esc}C_d(px)^2 \\ + \frac{2R_{esc}L_{esc}C_{esc}(px)^3}{6} + \frac{R_{esc}^3C_{esc}^2(px)^5}{120} + \frac{R_{lump}\mathrm{R}_{esc}C_{esc}^2(px)^3}{6} \\ + \frac{R_{esc}^2R_dC_dC_{esc}(px)^3}{6} + R_dC_d\left(L_{esc} + R_{lump}^2C_{esc}\right)(px)\end{array}\right] \tag{A2}$$

References

1. Chandel, R., Sarkar, S., Agarwal, R.P.: An analysis of interconnect delay minimization by low-voltage repeater insertion. Microelectron. J. **38**, 649–655 (2007)
2. Wen, W., Brongersma, S.H., Hove, M.V., Maex, K.: Influence of surface and grain-boundary scattering on the resistivity of copper in reduced dimensions. Appl. Phys. Lett. **84**, 3238–3240 (2004)
3. Goel, A.K.: High-speed VLSI Interconnections. Wiley-IEEE Press, New York (2007)
4. Li, H., Xu, C., Srivastava, N., Banerjee, K.: Carbon nanomaterials for next-generation interconnects and passives: physics, status, and prospects. IEEE Trans. Electron Devices **56**, 1799–1821 (2009)

5. McEuen, P.L., Fuhrer, M.S., Park, H.: Single-walled carbon nanotube electronics. IEEE Trans. Nanotechnol. **1**, 78–85 (2002)
6. Naeemi, A., Meindl, J.: Compact physical models for mutliwall carbon-nanotube interconnects. IEEE Electron Device Lett. **27**, 338–340 (2006)
7. Li, H., Banerjee, K.: High-frequency analysis of carbon nanotube interconnects and implications for on-chip inductor design. IEEE Trans. Electron Devices **56**, 2202–2214 (2009)
8. Nasiri, H., Rahim, F., Farshi, M.K.M.: Stability analysis in multiwall carbon nanotube bundle interconnects. Microelectron. Reliab. **52**, 3026–3034 (2012)
9. Fathi, D., Forouzandeh, B., Mohajerzadeh, S., Sarvari, R.: Accurate analysis of carbon nanotube interconnects using transmission line model. Micro Nano Lett. IET **4**, 116–121 (2009)
10. Li, H., Yin, W.Y., Banerjee, K., Mao, J.F.: Circuit modeling and performance analysis of multi-walled carbon nanotube interconnects. IEEE Trans. Electron Devices **55**, 1328–1337 (2008)
11. Das, D., Rahaman, H.: Analysis of crosstalk in single-and multiwall carbon nanotube interconnects and its impact on gate oxide reliability. IEEE Trans. Nanotechnol. **10**, 1362–1370 (2011)
12. Majumder, M.K., Narasimha Reddy, K., Kaushik, B.K.: Frequency response and bandwidth analysis of multi-layer graphene nanoribbon and multi-walled carbon nanotube interconnects. Micro Nano Lett. IET **9**, 557–560 (2014)
13. Fathi, D., Forouzandeh, B.: A novel approach for stability analysis in carbon nanotube interconnects. IEEE Electron Device Lett. **30**, 475–477 (2009)
14. International Technology Roadmap for Semiconductors, 2012. [Online]. Available: http://public.itrs.net/
15. Nagrath, I.J., Gopal, M.: Control Systems Engineering. Halsted Press, Sydney (1977)
16. Amore, D., Marcello Sarto, M.S., Tamburrano, A.: Fast transient analysis of next-generation interconnects based on carbon nanotubes. IEEE Trans. Electromagn. Comp. **52**, 496–503 (2010)

http://www.springer.com/978-981-10-1644-8

Proceedings of 2nd International Conference on Intelligent Computing and Applications
ICICA 2015
Deiva Sundari, P.; Dash, S.S.; Das, S.; Panigrahi, B.K. (Eds.)
2017, XIV, 694 p. 430 illus., 310 illus. in color.,
Softcover
ISBN: 978-981-10-1644-8